The Effectiveness of Global Thresholding Techniques in Segmenting Two-Phase Porous Media

Kokeb A. Abera, E.I.T., S.M. ASCE[1], Kalehiwot Nega Manahiloh, Ph.D., P.E., M.ASCE[2*], and Mohammad Motalleb Nejad, S.M. ASCE[3]

[1] Graduate Student, Dept. of Civil and Environmental Engineering, University of Delaware, 301 DuPont Hall, Newark, DE 19716, U.S.A.; e-mail: kabera@udel.edu
[2] Assistant Professor, Dept. of Civil and Environmental Engineering, University of Delaware, 301 DuPont Hall, Newark, DE 19716, U.S.A.; e-mail: knega@udel.edu
[3] Graduate Student, Dept. of Civil and Environmental Engineering, University of Delaware, 301 DuPont Hall, Newark, DE 19716, U.S.A.; e-mail: mohmtlb@udel.edu

* Corresponding Author

Abstract

The effectiveness of five global thresholding techniques, to accurately segment different geomaterials, was evaluated in this work. X-ray CT images -taken from two-phase pervious concrete, glass bead, and silica sand specimens- were analyzed for evaluating five chosen methods. The core algorithms for these methods were coded using a Matlab programming language and packaged into a standalone application software. Three hundred and thirty-five image slices were provided for the pervious concrete specimen and the cropped size of this specimen was approximately 68 mm in diameter. The method proposed by Kapur et al. (1985) yielded the best results qualitatively and quantitatively (e=0.28) to the laboratory and Image-Pro measured void ratios of 0.26 and 0.30, respectively. Eleven image slices were analyzed for a 10 mm in diameter glass bead specimen. Once again, the method proposed by Kapur et al. (1985) gave the best results with a void ratio of 0.91, as compared to the Image-Pro void ratio of 0.89. Ten image slices, with a cropped diameter of 4.48 mm, were used for the analysis of the silica sand specimen and the Otsu (1979) method was the most successful image segmentation technique, yielding a void ratio of 0.85 (Image-Pro e=0.77). From the results, it can be said that, no single image segmentation technique performs well over a wide range of material and that the performance of each image segmentation technique varies depending on the type and state of the analyzed media.

Keywords: Image processing, Segmentation, Thresholding, Void ratio, Porous media, X-ray CT.

Citation Information: please cite this work as follows

Abera, K.A., K.N. Manahiloh, and M. Motalleb Nejad, *The effectiveness of global thresholding techniques in segmenting two-phase porous media.* Construction and Building Materials, 2017. **142**: p. 256-267.

Link to published article: https://www.sciencedirect.com/science/article/pii/S0950061817304191

Introduction

Some of the most utilized segmentation techniques use the concept of thresholding. Thresholding techniques could be either bi-level or multi-level [1]. For bi-level thresholding, an image is segmented into two different regions. Pixels with gray values greater than a threshold value are classified as foreground (object) pixels and pixels with gray values less than a threshold value are classified as background pixels. On the other hand, in multi-level thresholding, a gray-level image is segmented into several distinct regions. Multi-level thresholding results in more than one threshold value for the image [2]. The field of image thresholding has been well researched, yielding many different models that can be used to achieve the same result of effectively segmenting an image.

Thresholding techniques can be categorized as global or local. Global thresholding is used when a chosen threshold value depends only on gray-level values and relates to the characteristics of pixels. There are numerous global thresholding techniques such as Otsu's method [3] that will be discussed further in this paper. The biggest issue that global thresholding methods face when utilizing an image's gray-level histogram is that not all features of interest form prominent peaks, in the image histogram, due to noise [1]. In the presented work, to ensure that the efficiency of the global thresholding techniques is not compromised, the images analyzed will be freed from any noise that could significantly affect the quality of the thresholding results.

Local thresholding techniques are applied when a threshold value depends on both the gray-level value and local property of a pixel. In other words, a different threshold value is determined for each pixel based on the grayscale information (e.g., range and variance) for the neighboring pixels [4]. This approach divides an image into several subregions and chooses a threshold for

each of these subregions. After such thresholds are applied, a gray-level filtering technique is used to eliminate discontinuous gray-levels among the subregions.

Global thresholding techniques, in segmenting two-phase porous media, have been discussed in the literature [3; 5-9]. From the vast range of global thresholding techniques, the Otsu (1979), Pun (1980), Kapur et al. (1985), Johannsen and Bille (1982), and Kittler and Illingworth (1986) methods are selected, based on their prior applicability success over a wide range of image types, and tested for their effectiveness in accurately segmenting geomaterials. Ensuing sections provide further details on these techniques, including the mathematical algorithms and theoretical concepts behind the selected methods.

Image acquisition and processing

Image acquisition

There are various types of images, such as magnetic resonance images (MRI), thermal images, and light intensity (visual) images. Light intensity images are the most commonly encountered type of images. As indicated in the name, light intensity images represent the variation of light intensity on the scene [2]. All images, regardless of type, can be viewed as digital images. A digital image is represented by a two-dimensional discrete function, f(x,y), which is digitized in both spatial coordinates and magnitude of feature value (e.g., light intensity, depth, and temperature intensity) [2]. The values of x and y in a discrete function represent row and column indices, respectively. A point marked by these indices is known as a pixel. The pixel equivalent in three-dimensional space is referred to as a voxel [10].

Images can be obtained through X-ray computed tomography (CT), which is an advanced imaging technique that allows for nondestructive and noninvasive imaging of specimens to

depict cross-sectional and three-dimensional internal structures [11]. Such a system is especially useful for highly porous materials [12]. There are numerous X-ray CT systems in the market today ranging from benchtop synchrotron microtomography scanners to industrial X-ray image acquisition systems. Figure 1 provides a general scheme for specimen installation in an X-ray CT chamber. X-ray beam, originating from an X-ray source, passes through a specimen and hits a detector where data that is useful in projecting the internal structural details of the scanned media is created. The specimen is rotated about an axis perpendicular to the beam and a detector processes attenuation coefficients of the X-rays as they emerge from the specimen. Each image slice represents a portion of the specimen and combining all of the slices together yields the virtual three-dimensional representation of the imaged specimen [13].

Image Segmentation

Image processing deals with utilizing algorithmic programs to identify and extract information from images. Almost all image processing tools convert an 8-bit or 16-bit image into its binary format after segmentation is performed. Binary images take smaller storage space, are easier to manipulate, and can be processed faster when a thresholding algorithm is applied. This binarization is what is commonly referred to as image segmentation and it represents the foundation for computer vision and object recognition. In image segmentation, the overall histogram of an image is partitioned into two regions, with the goal of separating objects of interest (i.e., the foreground) from the background [14]. The quality of the segmented image is controlled by how well the threshold that separates the foreground from the background is estimated.

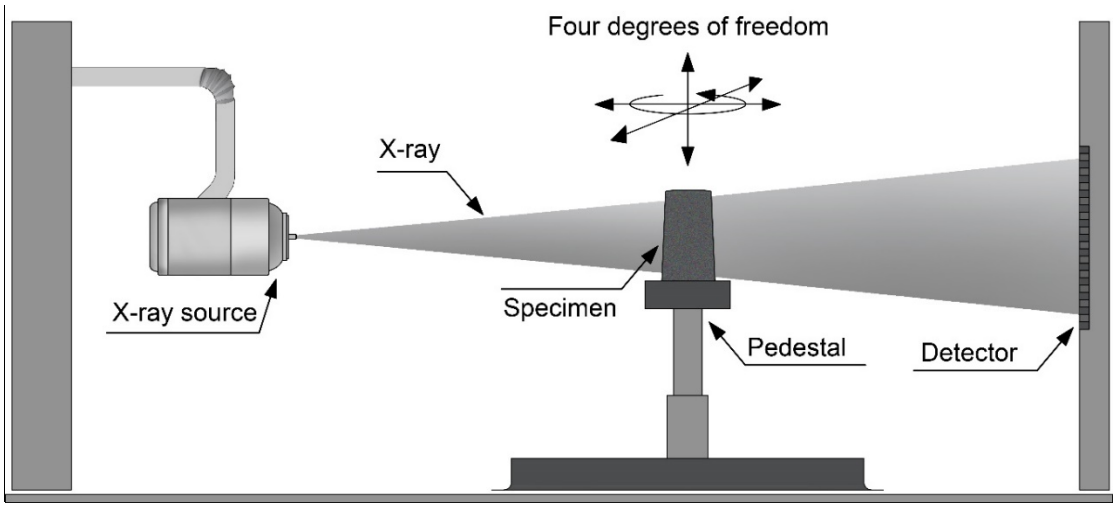

Figure 1. Schematic of Specimen Installation in X-ray CT Chamber

Advancements in image acquisition and processing technologies, over the last few decades, have allowed for tremendous growth in both the theory and application of image segmentation techniques. These techniques are very popular in many fields, such as medical [15], forensic [16, 17], and agricultural [18]. Scanned documents, including text, line drawings, or other graphics may be restored using the techniques of image segmentation if portions of these documents are degraded (e.g., aging resulting in ink fading) [4].

To further understand image segmentation, refer to Figure 2 which shows the general structure of an image segmentation system. The first step, preprocessing, is essential to eliminate any noise (random variation in pixel intensity) in the image before the segmentation step begins. For image preprocessing, color spaces within the image are transformed into specifically given color spaces for identifying different portions of an image [19]. The image is then smoothed through techniques such as a Gaussian filter [20] to minimize any noise. After applying a chosen image segmentation algorithm, post processing work entails of region merging, image marking, and

region extraction. This portion of the process combines unreasonably discontinuous regions to allow for a successfully segmented image [19].

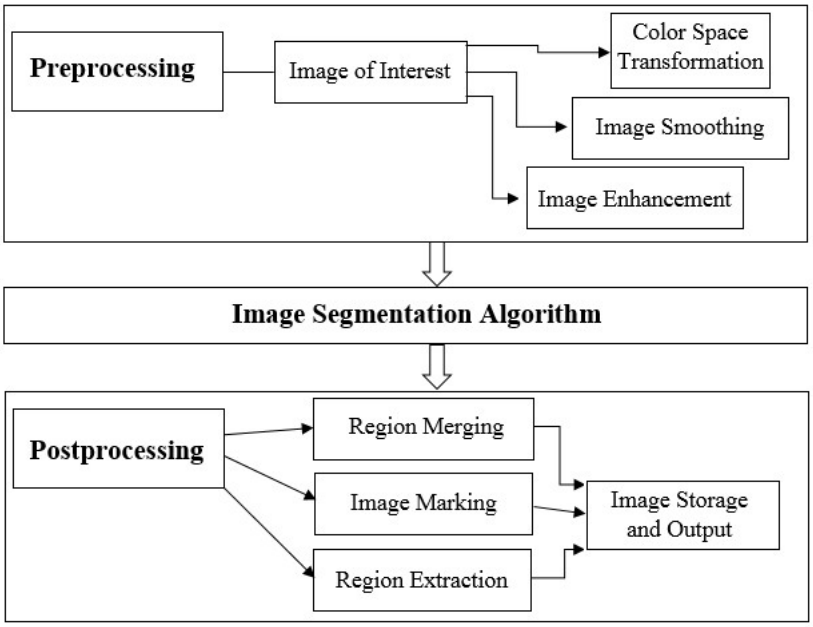

Figure 2. Image Segmentation System Structure (Yang and Kang 2009)

The three main categories of image segmentation are edge-based segmentation, special theory-based segmentation, and region-based segmentation [19]. Since the focus of this paper is on thresholding techniques, the region-based segmentation category is the one of interest (Table 1). The sub-classes of region-based segmentation are thresholding and region operating. The thresholding sub-class further divides into Otsu, optimal thresholding, and thresholding image techniques. The region operating sub-class divides into region growing, region splitting and merging, and image matching. In other words, the thresholding and region operating sub-classes can be categorized as global and local thresholding methods, respectively.

Table 1. Region-Based Segmentation Category (Yang and Kang 2009)

Sub-Classes		Interpretation
Thresholding	Otsu	Extract the objects from the background by setting reasonable gray threshold Ts for image pixels.
	Optimal thresholding	
	Thresholding image	
Region operating	Region growing	Partition an image into regions that are similar according to given criteria, such as gray character, color character, texture character, etc.
	Region splitting and merging	
	Image matching	

Image segmentation is a very useful tool for obtaining and analyzing the properties of porous media, such as soils, rocks, concrete, and glass. Rather than performing laboratory experiments on a physical specimen of a two-phase porous media, images of the media can be used in conjunction with thresholding techniques, to quickly and accurately yield material properties such as void ratio (e).

Implementation of Thresholding Techniques

Through previously conducted literature review, five global thresholding techniques, namely Otsu (1979), Pun (1980), Kapur et al. (1985), Johannsen and Bille (1982), and the Kittler and Illingworth (1986) methods, were chosen for application to multiple porous media. Table 2 lists some of the commonly applied thresholding techniques for two-dimensional “slice-by-slice” processing of porous media, which also includes the five implemented techniques of this study.

Table 2. Commonly Applied Thresholding Techniques for Porous Media

Technique	Material	Thresholding Technique
Baveye et al. (2010), [21]	Soil	3D Thresholding
Carminati et al. (2007), [22]	Soil	3D Thresholding
Culligan et al. (2006), [23]	Glass Beads	3D Thresholding
Jassogne et al. (2007), [24]	Soil	2D Thresholding
Johannsen and Bille (1982), [7]	-	2D Thresholding
Kaestner et al. (2008), [25]	Soil	3D Thresholding
Kapur et al. (1985), [6]	-	2D Thresholding
Kittler and Illingworth (1986), [8]	-	2D Thresholding
Kurita et al. (1992), [26]	Glass Beads, Sandstone	2D Thresholding
Lee et al. (2008), [27]	Soil	2D Thresholding
Nunan et al. (2006), [28]	Aggregates	2D Thresholding
Ojeda-Magaña et al. (2014), [29]	Soil	3D Thresholding
Otsu (1979), [3]	-	2D Thresholding
Pun (1980), [5]	-	2D Thresholding
Ridler et al. (1978), [30]	Glass Beads	2D Thresholding
Schaap et al. (2007), [31]	Glass Beads	3D Thresholding
Schlüter et al. (2010), [32]	Soil	2D Thresholding
Van Geet et al. (2003), [33]	Limestone, Sandstone	3D Thresholding
Vogel et al. (2005), [34]	Sintered Glass	3D Thresholding
Wildenschild et al. (2002), [35]	Sand	3D Thresholding

Each of the five chosen algorithms were programmed with MATLAB [36]. A subroutine that calculates and reports the void ratio from X-ray CT images was created and applied. Generally, the subroutine reads an image slice, crops it to a circle of appropriate size (so that the number of pixels are not over- or under-estimated), segments it by applying a chosen thresholding technique, and counts the number of void and solid pixels in the segmented image. Void ratio is determined by dividing the number of void pixels by the number of solid pixels. Since the scanned images represent a two-phase system, the total number of pixels are composed of air and solids. Once all of the image slices are processed, results are combined and reported as the void ratio of the specimen.

For computational efficiency, each analyzed image was converted to an 8-bit image, meaning that the grayscale pixel intensities range from 0-255, where pixels closer to the 0 end are colored black and pixels closer to the 255 end are white. For MATLAB coding purposes, this range is taken to be from 1-256. Since the segmentation program is applied for two-phase images, void pixels are equal to air pixels. Therefore, any pixels less than a threshold value are black which corresponds to air and any pixels greater than a threshold value are white which corresponds to solids. In the images analyzed in this study, the process of reducing the bit depth from 16-bit to 8-bit does not result in a significant loss of information. This could be attributed to the fact that the specimens were made of “larger” sized granular media and important details were well preserved in the 8-bit images.

Otsu (1979) calculates optimal threshold through separability of the two classes, namely the foreground and background, by minimizing within-class variance or maximizing between-class variance. Optimal threshold is located where the summation of the foreground and background spreads are at a minimum [3]. Equations 1-4 are used for this method, where the optimal threshold value (t) is taken as the pixel value yielding the maximum value from Equation 4.

$$mean = \frac{\sum_{i=1}^{c} i * p_i}{c} \tag{1}$$

$$meanli = \frac{\sum_{i=1}^{t-1} i * p_i}{c} \tag{2}$$

$$meangi = \frac{\sum_{i=t}^{c} i * p_i}{c} \tag{3}$$

$$t = \arg\max\{\sum_{i=1}^{t-1} p_i * \{meanli - mean\}^2 + \sum_{i=t}^{c} p_i * \{meangi - mean\}^2\} \tag{4}$$

In the above equations, c is the highest possible pixel value in an image (here, since 8-bit images are processed in MATLAB, the highest possible value is 256); i represents a pixel value within the range of one up to c; p represents the individual pixel frequencies; mean, meanli, and meangi represent the mean of an image's pixel intensities ranging from one to c, one to *t*-1, and *t* to c, respectively.

In the Pun (1980) method, an assumption is made that the relationship between the numbers of pixels at a specific gray-level is statistically independent from the number of pixels at a nearby gray-level. Realistically, this assumption is not necessarily true, but is taken to be factual since this thresholding algorithm's derivation is greatly simplified while providing reasonable results [5]. Equations 5-8 are utilized for the Pun (1980) method, where the optimal threshold value (*t*) is determined when the criteria set by Equation 8 is achieved.

$$p_i = \frac{n(i)}{n} \tag{5}$$

$$\sum_{i=1}^{m} p_i \geq 0.5 \tag{6}$$

$$\alpha = \frac{\sum_{i=1}^{m} p_i * \log_e p_i}{\sum_{i=1}^{c} p_i * \log_e p_i} \tag{7}$$

$$\sum_{i=1}^{t} p_i = \begin{cases} \alpha, & \alpha > 0.5 \\ 1-\alpha, & \alpha \leq 0.5 \end{cases} \tag{8}$$

In Equations 5-8, p_i is the probability of occurrence of gray-level i; n(i) corresponds to the total number of pixels at a specific pixel value i; n represents the total number of pixels in an image; m is the smallest pixel value that satisfies Equation 6; α is the anisotropy coefficient representing

the ratio of the average quantity of information of white and black pixels; c is the highest possible pixel value in an image.

The Kapur et al. (1985) method first derives two probability distributions (foreground and background) from the original gray-level distribution of an image and then determines the entropies associated with each distribution. The optimal threshold is taken as the gray-level that has the greatest summation of the two entropies [6]. Equations 9-15 represent this algorithm, where the optimal threshold value (*t*) refers to the pixel value that results in the maximum value of Equation 15.

$$p_i = \frac{n(i)}{n} \tag{9}$$

$$H_i = -\sum_{i=1}^{c} p_i * \log_e p_i \tag{10}$$

$$P_t = \sum_{i=1}^{t} p_i \tag{11}$$

$$H_t = -\sum_{i=1}^{t} p_i * \log_e p_i \tag{12}$$

$$H_a = \log_e P_t + \frac{H_t}{P_t} \tag{13}$$

$$H_b = \log_e (1 - P_t) + \frac{(H_i - H_t)}{(1 - P_t)} \tag{14}$$

$$t = \arg\max\{H_a + H_b\} \tag{15}$$

In the above equations, p_i is the probability of occurrence of gray-level i; c is the highest possible pixel value in an image; H_a and H_b represent the two probability distributions derived from the original gray-level distribution of the image.

The fourth algorithm, Johannsen and Bille (1982), is represented by Equations 16-18. Through utilizing the entropy of the gray-level histogram of an image, this method determines the optimal threshold value by dividing the set of gray-levels into foreground and background classes, in order to minimize the interdependence between them [9]. The minimum value produced from Equation 18 corresponds to the optimal threshold value (n^*).

$$S(n) = \log_e(\sum_{i=1}^{n} p_i) - \frac{1}{\sum_{i=1}^{n} p_i} * [p_n * \log_e p_n + (\sum_{i=1}^{n-1} p_i) * \log_e(\sum_{i=1}^{n-1} p_i)] \quad (16)$$

$$\bar{S}(n) = \log_e(\sum_{i=n}^{c} p_i) - \frac{1}{\sum_{i=n}^{c} p_i} * [p_n * \log_e p_n + (\sum_{i=n+1}^{c} p_i) * \log_e(\sum_{i=n+1}^{c} p_i)] \quad (17)$$

$$n^* = \arg\min(S(n) + \bar{S}(n)) \quad (18)$$

For Equations 16-18, p_i corresponds to the probability of occurrence of gray-level i; p_n represents the probability of occurrence of the pixel value following the one being analyzed (e.g., if i=25, p_n represents the probability for pixel value 26); n = *t*+1; c is the highest possible pixel value in an image; S(n) and $\bar{S}$(n) represent the two parts that the set of gray-levels are divided into.

The fifth and final method that will be used for analysis is the Kittler and Illingworth (1986) method. The Kittler and Illingworth (1986) method determines the optimal threshold value by viewing the gray-level histogram as an estimation of the probability density function representing the gray-levels of the foreground and background pixels in an image. This method assumes that these two categories of pixels are normally distributed with priori probability, mean, and standard deviation [9]. The algorithm for the Kittler and Illingworth (1986) method is presented by Equations 19-26, where the optimal threshold value (*t*) is the minimum value of the criterion function of Equation 26.

$$P_1 = \sum_{j=1}^{t} P_j \tag{19}$$

$$P_2 = \sum_{j=t+1}^{c-1} P_j$$

(20)

$$\mu_1 = \frac{(\sum_{j=1}^{t} P_j * j)}{P_1} \tag{21}$$

$$\mu_2 = \frac{(\sum_{j=t+1}^{c-1} P_j * j)}{P_2} \tag{22}$$

$$\sigma_1^{\,2} = \frac{\sum_{j=1}^{t} (j-\mu_1)^2 \times P_j}{P_1} \tag{23}$$

$$\sigma_2^{\,2} = \frac{\sum_{j=t+1}^{c-1} (j-\mu_2)^2 \times P_j}{P_2} \tag{24}$$

$$J = 1 + 2*(P_1 * \log_e \sigma_1 + P_2 * \log_e \sigma_2) - 2*(P_1 * \log_e P_1 + P_2 * \log_e P_2) \tag{25}$$

$$t^* = \arg\min(J) \tag{26}$$

For Equations 19-26, P_1 and P_2, μ_1 and μ_2, σ_1^2 and σ_2^2, and σ_1 and σ_2 represent the priori probability, mean, variance, and standard deviation of the foreground and background pixels, respectively; c is the highest possible pixel value in an image.

Results and Discussion

The five thresholding techniques described in the preceding section were applied to X-ray CT images obtained for three different specimens. These specimens were composed of pervious

concrete, glass bead, and silica sand. In order to qualitatively analyze the results of the five techniques, and present that discussion here, the segmentation results of each method is represented by the first image slice for the image set of each specimen.

The subroutines of the five thresholding techniques were deployed as a standalone executable software program, thus removing the need for MATLAB. Besides allowing non-MATLAB users the opportunity to utilize these subroutines, creating a standalone program allows for all of the methods to be neatly displayed on one screen, rather than running multiple scripts. The images to undergo segmentation must be cropped to ensure that calculations are performed only for the specimen. In other words, images are composed of pixels whose information is stored in a matrix that can either be square-shaped or rectangular-shaped. If a specimen is circular-shaped, portions of the four corners of the image would not include any of the specimen, as seen in Figure 3, which represents the first image slice of the pervious concrete specimen.

If the image slice in Figure 3 is not cropped, the thresholding algorithms would mistake these black corners as air, thus greatly overestimating the specimen's void ratio. Image slice renderings could include the container that the specimen was scanned in and a scale for the sizes of the particles, depending on how the specimens were scanned and how the image slices were presented. Regardless, these inclusions would result in inaccurate results, further solidifying the need for image cropping. Automatic image cropping on the basis of pixel information would not always be accurate, especially if a scale is included for each image slice and if the soil specimen is not centered in the image.

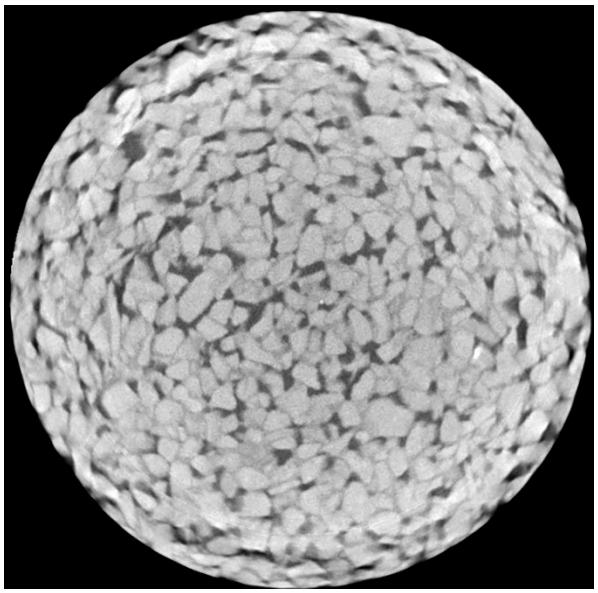

Figure 3. First Scanned Image Slice of Pervious Concrete Specimen

The pervious concrete specimen was originally 100 mm in diameter and was newly prepared in a laboratory setting. Three hundred and thirty-five image slices were obtained for this specimen through X-ray CT scanning. The laboratory measured gravimetric void ratio was 0.26. Figure 4 shows the first image slice with the applied manual crop as displayed in the standalone software developed as part of this study. The calibrated size of this cropped specimen was approximately 68 mm in diameter.

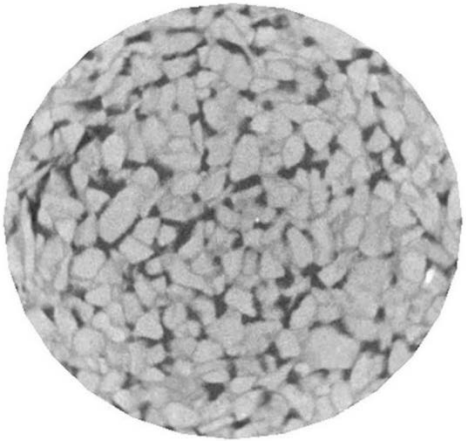

Figure 4. First Cropped Image Slice of Pervious Concrete Specimen

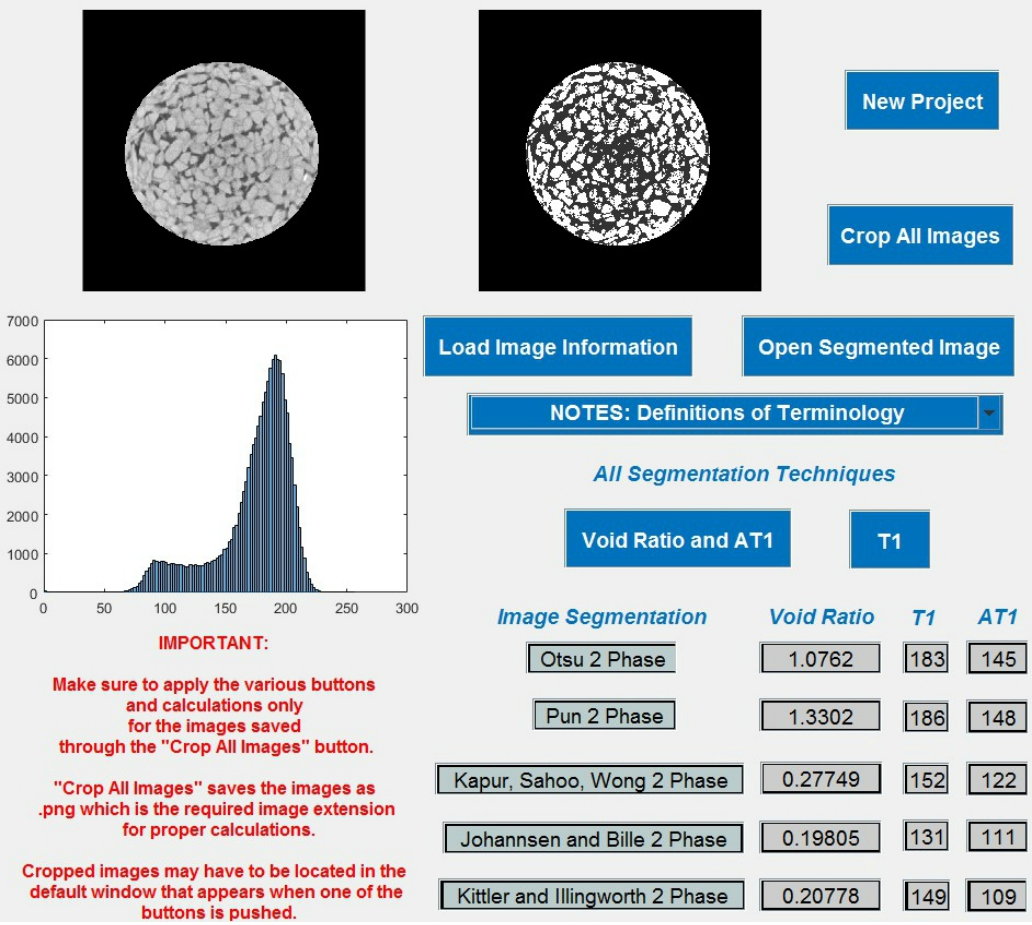

Figure 5. Pervious Concrete Results of Thresholding Techniques (Displayed Image Slice Segmented with the Otsu (1979) Method)

Figure 5 above shows the quantitative results from the applied thresholding techniques. The void ratio, threshold value for the first image slice (T1), and the average threshold value (AT1) for the set of image slices per method is displayed in the figure. Also, for visual purposes, the figure depicts the cropped image of the original first image slice, its gray-level histogram, and the resulting segmented image with the Otsu (1979) method applied. To assist with qualitative analyses, Figure 6 presents the segmentation of the first image slice per thresholding method.

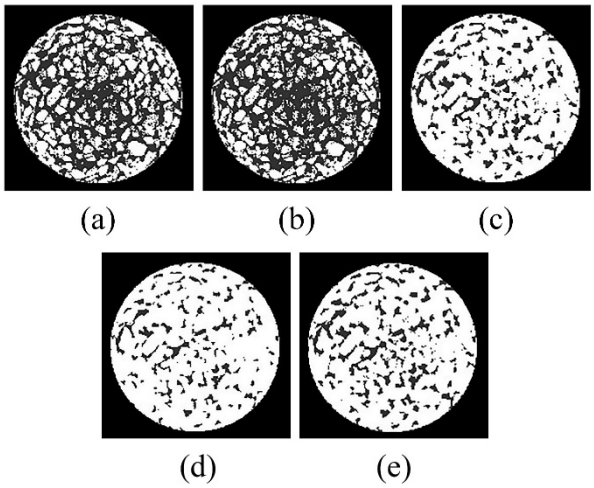

Figure 6. Segmented Pervious Concrete Slice with Different Thresholding Methods Applied: (a) Otsu (1979) Method, (b) Pun (1980) Method, (c) Kapur et al. (1985) Method, (d) Johannsen and Bille (1982) Method, (e) Kittler and Illingworth (1986) Method

The void ratio for Otsu (1979), Pun (1980), Kapur et al. (1985), Johannsen and Bille (1982), and the Kittler and Illingworth (1986) methods were 1.076, 1.33, 0.28, 0.20, and 0.21, respectively. As previously mentioned, the laboratory measured void ratio was found to approximately be 0.26. For the first image slice, the Pun (1980) method had the highest threshold value (T1=186), followed by Otsu (1979) (T1=183), Kapur et al. (1985) (T1=152), Kittler and Illingworth (1986) (T1=149), and the Johannsen and Bille (1982) methods (T1=131). On average, the threshold values for the entire image set for these five techniques were 148, 145, 122, 109, and 111, respectively.

From a quantitative standpoint, for the pervious concrete specimen, the results from Otsu (1979) and the Pun (1980) methods were the least accurate of the five thresholding techniques. Qualitatively speaking, the segmentation of this image slice by these two methods eroded away too much of the solid particles, more so with the Pun (1980) method. The average threshold values for these methods were very close to one another and helped validate this argument. Since

their algorithms determined the thresholds to be this high, the methods yielded unrealistic void counts for the specimen. Therefore, it can be deduced that an acceptable segmentation technique must have an average threshold value much lower than what was seen with these two methods. The void ratios from Kapur et al. (1985), Johannsen and Bille (1982), and the Kittler and Illingworth (1986) methods were very similar to one another. Relatively speaking, the best segmentation technique for this image set was the Kapur et al. (1985) method. Quantitatively, this technique's void ratio was the closest to the laboratory measured void ratio. For further validation, the image processing program, Image-Pro®, yielded a void ratio of 0.30 which was also relatively close to the result from the Kapur et al. (1985) method. Image-Pro was selected as a validation measure because of the degree of control users can have in deciding the optimum threshold for the image slices analyzed. Once the appropriate threshold is identified, on a number of slices, automated macros are run to analyze the whole image stack. Qualitatively, this method came the closest to accurately capturing the size and shape of the solid particles in the original image, whereas the other two methods had the solid particles being more filled and widened.

The original glass bead specimen was 10 mm in diameter and eleven image slices (first cropped image slice depicted as Figure 7) were obtained for this specimen through X-ray CT scanning. The cropped images contained the entire specimen, so the diameter remained as 10 mm. Figure 8 provides the quantitative results of the applied thresholding methods (first image slice used for T1) and the qualitative results of the first image slice with the Otsu (1979) method applied. Figure 9 presents the segmentation of the first image slice with each thresholding method applied.

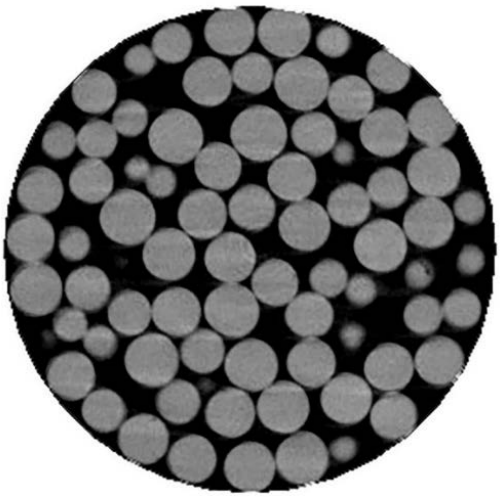

Figure 7. First Cropped Image Slice of Glass Bead Specimen

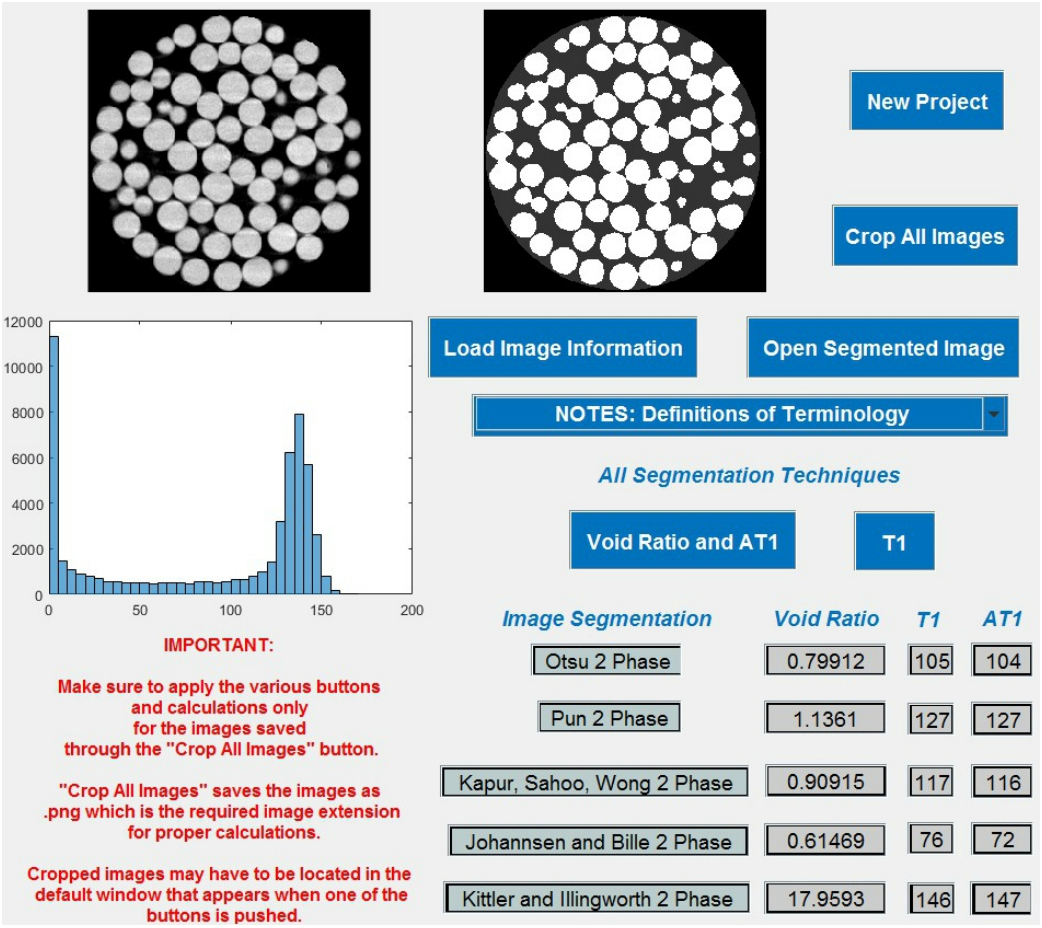

Figure 8. Glass Bead Results of Thresholding Techniques (Displayed Image Slice Segmented with the Otsu (1979) Method)

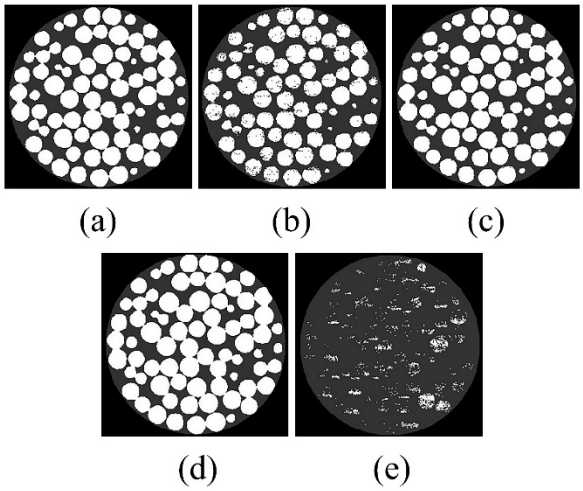

Figure 9. Segmented Glass Bead Image Slice with Different Thresholding Methods Applied: (a) Otsu (1979) Method, (b) Pun (1980) Method, (c) Kapur et al. (1985) Method, (d) Johannsen and Bille (1982) Method, (e) Kittler and Illingworth (1986) Method

Quantitatively, the void ratio of 17.96 obtained through the Kittler and Illingworth (1986) method was very inaccurate. From Figure 9e, it can be seen that this technique poorly segmented the image, treating the majority of solid pixels as void pixels. The threshold value of 146 for the first image slice and the average threshold value of 147 for the set of image slices were far too large. The Johannsen and Bille (1982) method yielded the smallest void ratio of 0.61, followed by Otsu (1979) (e=0.80), Kapur et al. (1985) (e=0.91), and the Pun (1980) methods (e=1.14). The corresponding threshold values for the first image slice were 76, 105, 117, and 127, respectively. The average threshold values for the set of image slices were 72, 104, 116, and 127, respectively. For a basis of comparison, Image-Pro yielded a void ratio of 0.89. Thus, the Kapur et al. (1985) method provided the best segmentation, quantitatively.

By qualitatively analyzing the segmentation results, it can immediately be seen that Pun (1980) and the Kittler and Illingworth (1986) methods yielded unacceptable segmentations. The specimen segmented by the Pun (1980) method had small black dots scattered across the glass

beads, indicating more voids and hence a higher threshold value than what is realistic. The Kittler and Illingworth (1986) method yielded the highest threshold value of all the techniques which explained why this method barely captured any of the glass beads. For the Johannsen and Bille (1982) method, the glass beads were slightly too filled and widened. This was visually identifiable since this segmentation resulted in the formation of contact points where gaps should have resided. Otsu (1979) and the Kapur et al. (1985) methods were the two best segmentation options which also had void ratios closest to the Image-Pro void ratio. The Otsu (1979) method resulted in unwanted contact points between the glass beads in various locations of the specimen, although not as profound as with the Johannsen and Bille (1982) method. So, overall, the Kapur et al. (1985) method yielded the best results quantitatively and qualitatively for the glass bead specimen.

The third and last specimen analyzed was silica sand with a specimen diameter of 6.35 mm. Ten image slices were utilized (first cropped image slice represented by Figure 10) for the analysis. The specimen was cropped to a diameter of 4.48 mm. Figure 11 shows the results from the standalone program with T1 calculated for the first image slice and the segmentation of this slice displayed with the Otsu (1979) method as well. Figure 12 presents the segmentation of the first image slice with each thresholding method applied.

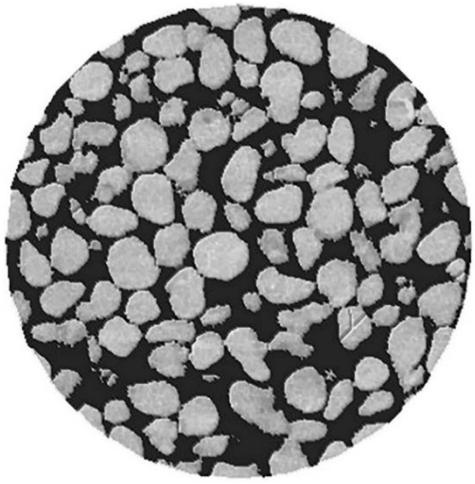

Figure 10. First Cropped Image Slice of Silica Sand Specimen

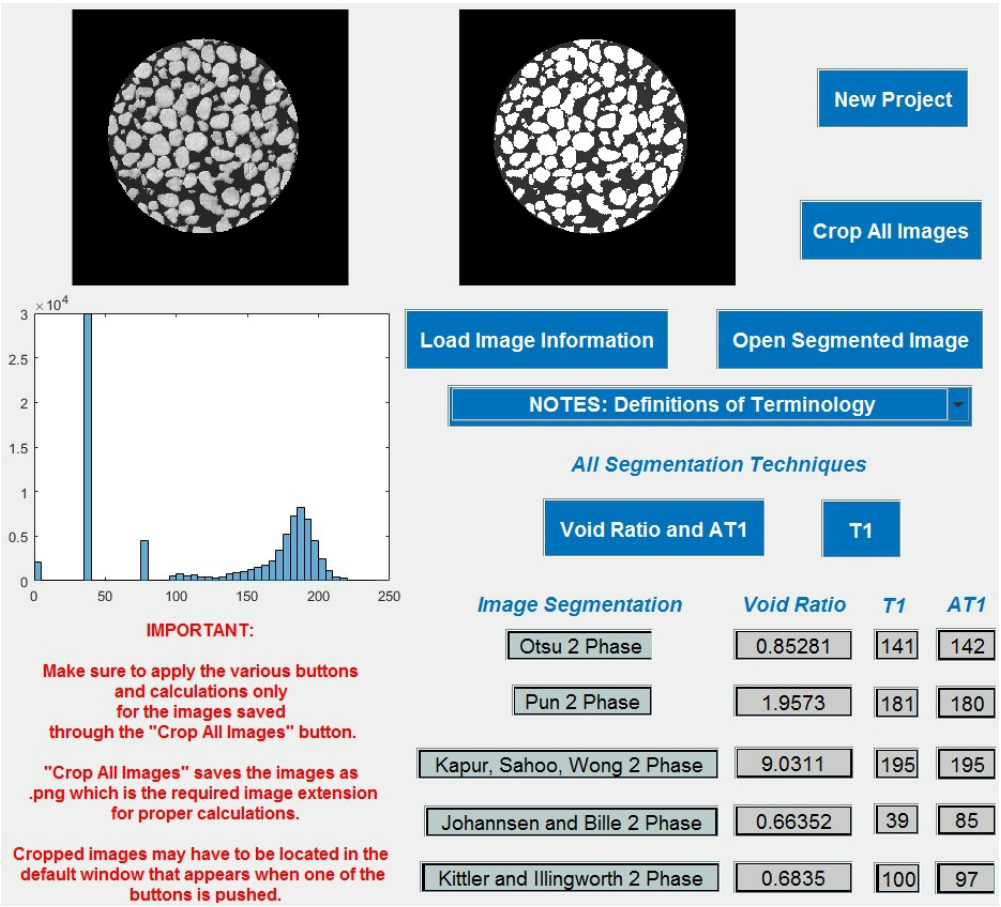

Figure 11. Silica Sand Results of Thresholding Techniques (Displayed Image Slice Segmented with the Otsu (1979) Method)

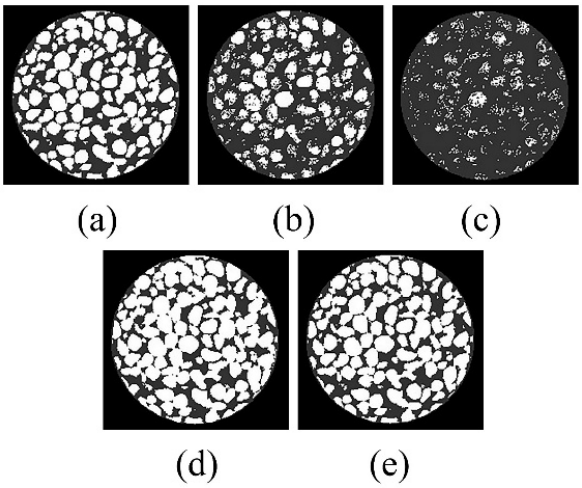

Figure 12. Segmented Silica Sand Image Slice with Different Thresholding Methods Applied: (a) Otsu (1979) Method, (b) Pun (1980) Method, (c) Kapur et al. (1985) Method, (d) Johannsen and Bille (1982) Method, (e) Kittler and Illingworth (1986) Method

From Figure 11, the void ratio of 9.031 obtained through the Kapur et al. (1985) method seems too high, meaning that the corresponding threshold values of 195, for the first image slice and the whole set of image slices, were not realistic. This value suggested that the original silica sand specimen was significantly composed of more air than sand particles, which was not the case. For the other image segmentation techniques, the method with the highest void ratio was the Pun (1980) method (e=1.96), followed by Otsu (1979) (e=0.85), Kittler and Illingworth (1986) (e=0.68), and the Johannsen and Bille (1982) (e=0.66) methods. The threshold values for the first image slice for these methods were 181, 141, 100, and 39, respectively. The average threshold values for the four methods were 180, 142, 97, and 85, respectively. Comparing to the void ratio of 0.77 that was obtained from Image-Pro, the Otsu (1979) method was the best segmentation technique for the silica sand specimen.

Qualitatively, starting with the Pun (1980) method, the segmented image slice in Figure 12b shows that the solid particles are too eroded away, in comparison to the original image slice. In

other words, the chosen threshold value was too high since the segmented image visually contained too much air. The Johannsen and Bille (1982) method had the lowest threshold value which caused the solid particles to be too filled (Figure 12d). Lastly, Otsu (1979) and the Kittler and Illingworth (1986) methods provided similar qualitative results. However, the Otsu (1979) method was more capable of capturing the visible cracks in the silica sand particles. As a result, the Otsu (1979) method was chosen as the best image segmentation technique for the silica sand specimen.

Table 3 provides a summary of the final void ratio results for the porous media analyzed in this study. Tables 4-6 provide statistical descriptors and comparisons of the five techniques for each of the porous media analyzed. Note that for Table 5 the Kittler and Illingworth (1986) method was excluded from the statistical comparison due to the produced void ratio being a wild outlier. The same reasoning applied for why the Kapur et al. (1985) method was not included in Table 6. The results of these tables collectively show that the methods as a whole work best for the glass bead specimen due to this specimen having the lowest coefficient of variation. This is followed by the silica sand specimen and the pervious concrete specimen. Individually, the application of the Kapur et al. (1985) method to the glass bead specimen yielded the least segmentation error (1.71%). Contrarily, the best segmentation technique with the greatest segmentation error (10.49%) was the Otsu (1979) method for the silica sand specimen.

Table 3. Final Void Ratio Results for the Porous Media Specimens

Porous Media	Best Segmentation Technique	Chosen Technique's Void Ratio	Image-Pro Void Ratio	Percent Error
Pervious Concrete	Kapur et al. (1985)	0.28	0.30	6.89%
Glass Bead	Kapur et al. (1985)	0.91	0.89	1.71%
Silica Sand	Otsu (1979)	0.85	0.77	10.49%

Table 4. Statistical Results and Comparisons for the Pervious Concrete Specimen[*1]

Porous Media	Image Segmentation Technique	Void Ratio	Error	Standard Deviation	Coefficient of Variation (CV)
Pervious Concrete	Otsu (1979)	1.076	0.61	0.46	74.25%
	Pun (1980)	1.33	1.065		
	Kapur et al. (1985)	0.28	0.00042		
	Johannsen and Bille (1982)	0.20	0.0010		
	Kittler and Illingworth (1986)	0.21	0.0081		
	Image-Pro	0.30	_____		

Table 5. Statistical Results and Comparisons for the Glass Bead Specimen[*1]

Porous Media	Image Segmentation Technique	Void Ratio	Error	Standard Deviation	Coefficient of Variation (CV)
Glass Bead	Otsu (1979)	0.80	0.0090	0.19	21.82%
	Pun (1980)	1.14	0.059		
	Kapur et al. (1985)	0.91	0.00024		
	Johannsen and Bille (1982)	0.61	0.078		
	Image-Pro	0.89	_____		

Table 6. Statistical Results and Comparisons for the Silica Sand Specimen[*1]

Porous Media	Image Segmentation Technique	Void Ratio	Error	Standard Deviation	Coefficient of Variation (CV)
Silica Sand	Otsu (1979)	0.85	0.0066	0.54	51.49%
	Pun (1980)	1.96	1.41		
	Johannsen and Bille (1982)	0.66	0.012		
	Kittler and Illingworth (1986)	0.68	0.0078		
	Image-Pro	0.77	_____		

Conclusions

[1] Comparisons made relative to Image-Pro Plus determined void ratios.

Five automatic thresholding techniques, Otsu (1979), Pun (1980), Kapur et al. (1985), Johannsen and Bille (1982), and the Kittler and Illingworth (1986) methods, were chosen for image segmentation of two-phase porous media. Since these techniques dealt with two-phase image segmentation, one threshold value was determined to separate the foreground/objects and background/air classes from each other. Pixels less than a threshold value were referred to as void/air pixels that were colored black and pixels greater than a threshold value were referred to as solid pixels colored white. The algorithms for the five chosen thresholding techniques were coded in MATLAB to ultimately determine material properties such as void ratio (e) for image slices obtained from an X-ray CT device.

The determination of an optimal threshold value varied from technique to technique due to differences in mathematical algorithms. The Otsu (1979) method found the optimal threshold value through minimization of the within-class variance of the foreground and background classes of an image's gray-level histogram. The Pun (1980) method made the assumption that pixel information was statistically independent from one another. The Kapur et al. (1985) method chose the optimal threshold value through determining two probability distributions representing the foreground and background classes. The Johannsen and Bille (1982) method determined the threshold value to be the gray-level pixel value resulting in the minimal interdependence between the foreground and background classes. Lastly, the Kittler and Illingworth (1986) method considered the gray-level histogram to be an estimation of the probability density function of the foreground and background classes. This method assumed that the pixels within these two classes were normally distributed and thus calculated the threshold value through utilization of pixel probability, mean, and standard deviation.

In order to analyze the effectiveness of the thresholding techniques, the techniques were applied to pervious concrete, glass bead, and silica sand specimens. Three hundred and thirty-five image slices were provided for the pervious concrete specimen and the cropped size of this specimen was approximately 68 mm in diameter. The method proposed by Kapur et al. (1985) yielded the best results qualitatively and quantitatively (e=0.28) to the laboratory measured void ratio of 0.26 and the Image-Pro void ratio of 0.30. Eleven image slices were utilized for the 10 mm in diameter glass bead specimen. Once again, the method proposed by Kapur et al. (1985) gave the best results with a void ratio of 0.91, as compared to the Image-Pro void ratio of 0.89. Ten image slices with a cropped diameter of 4.48 mm were used for the analysis of the silica sand specimen and the Otsu (1979) method was the most successful image segmentation technique, yielding a void ratio of 0.85 (Image-Pro e=0.77).

Interestingly, the results of the applied image segmentation techniques for the three porous media specimens do not follow a specific type of trend. The analysis of the pervious concrete specimen showed that the Kapur et al. (1985) method was the best technique whereas the Pun (1980) method was the least accurate for this specimen. For the glass bead specimen, the Kapur et al. (1985) method proved most successful and the Kittler and Illingworth (1986) method was clearly the least successful. Lastly, the segmentation of the silica sand specimen was best captured by the Otsu (1979) method and was least captured by the Kapur et al. (1985) method (in contrast with the pervious concrete and glass bead specimens). Therefore, it was difficult to make pre-analysis assumptions on which of the five techniques performed the best; the performance of the techniques varied based on the type of porous media analyzed. Regardless, the five evaluated image segmentation techniques could very well open up more possibilities in the field of two-phase image segmentation of porous media in the near future.

Acknowledgments

This work was supported by the Center for Advanced Infrastructure and Transportation (CAIT) through the national University Transportation Centers (UTC) Program.

References

[1] Leedham, G., Yan, C., Takru, K., Tan, J. H. N., & Mian, L. (2003). Comparison of some thresholding algorithms for text/background segmentation in difficult document images. *Proceedings of the International Conference on Document Analysis and Recognition, ICDAR*, *2003–January* (Icdar), 859–864. https://doi.org/10.1109/ICDAR.2003.1227784

[2] Pal, N. R., & Pal, S. K. (1993). A review on image segmentation techniques. *Pattern Recognition*, *26*(9), 1277–1294. https://doi.org/10.1016/0031-3203(93)90135-J

[3] [3] Otsu, N. (1979). A threshold selection method from gray-level histograms. *IEEE Transactions on Systems, Man, and Cybernetics*, *9*(1), 62–66. https://doi.org/10.1109/TSMC.1979.4310076

[4] Singh, T. R., Roy, S., Singh, O. I., Sinam, T., and Singh, K. M. (2011). "A new local adaptive Thresholding technique in Binarization." *International Journal of Computer Science Issues*, 8(2), 271-277.

[5] Pun, T. (1980). A new method for grey-level picture thresholding using the entropy of the histogram. *Signal Processing*, *2*(3), 223–237. https://doi.org/10.1016/0165-1684(80)90020-1

[6] Kapur, J. N., Sahoo, P. K., & Wong, A. K. C. (1985). A new method for gray-level picture thresholding using the entropy of the histogram. *Computer Vision, Graphics, and Image Processing*, *29*(1), 140. https://doi.org/10.1016/0734-189X(85)90125-2

[7] Johannsen, G., and Bille, J. (1982). "A threshold selection method using information measures." *6th International Conference on Pattern Recognition*, 140-143.

[8] Kittler, J., & Illingworth, J. (1986). Minimum error thresholding. *Pattern Recognition*, *19*(1), 41–47. https://doi.org/10.1016/0031-3203(86)90030-0

[9] Sahoo, P. K., Soltani, S., & Wong, A. K. C. (1988). A survey of thresholding techniques. *Computer Vision, Graphics and Image Processing*, *41*(2), 233–260. https://doi.org/10.1016/0734-189X(88)90022-9

[10] Manahiloh, K. N., Muhunthan, B., Kayhanian, M., & Gebremariam, S. Y. (2012). X-Ray Computed Tomography and Nondestructive Evaluation of Clogging in Porous Concrete Field Samples. *Journal of Materials in Civil Engineering*, *24*(8), 1103–1109. https://doi.org/10.1061/(ASCE)MT.1943-5533.0000484

[11] Iassonov, P., Gebrenegus, T., & Tuller, M. (2009). Segmentation of X-ray computed tomography images of porous materials: A crucial step for characterization and quantitative analysis of pore structures. *Water Resources Research*, *45*(9), 1–12. https://doi.org/10.1029/2009WR008087

[12] Maire, E., Colombo, P., Adrien, J., Babout, L., & Biasetto, L. (2007). Characterization of the morphology of cellular ceramics by 3D image processing of X-ray tomography. *Journal of the European Ceramic Society*, *27*(4), 1973–1981. https://doi.org/10.1016/j.jeurceramsoc.2006.05.097

[13] Madra, A., Hajj, N. El, & Benzeggagh, M. (2014). X-ray microtomography applications for quantitative and qualitative analysis of porosity in woven glass fiber reinforced thermoplastic. *Composites Science and Technology*, *95*, 50–58. https://doi.org/10.1016/j.compscitech.2014.02.009

[14] Kohler, R. (1981). A segmentation system based on thresholding. *Computer Graphics and Image Processing, 15*(4), 319–338. https://doi.org/10.1016/S0146-664X(81)80015-9

[15] Sund, R., and Eilertsen, K. (2003). "An algorithm for fast adaptive image binarization with applications in radiotherapy imaging." *IEEE Transactions on Medical Imaging*, 22, 22-28.

[16] Russ, J. C. (2015). *Forensic Uses of Digital Imaging, Second Edition*, CRC Press.

[17] Wen, C. Y., and Chen, J. K. (2004). "Multi-resolution image fusion technique and its application to forensic science." *Forensic Science International*, 140(2–3), 217-232.

[18] Abdullah, S. L. S., Hambali, H., & Jamil, N. (2012). Segmentation of natural images using an improved thresholding-based technique. *Procedia Engineering*, *41*(Iris), 938–944. https://doi.org/10.1016/j.proeng.2012.07.266

[19] Yang, Q., & Kang, W. (2009). General Research on Image Segmentation Algorithms. *I.J. Image, Graphics and Signal Processing*, *1*(October), 1–8. https://doi.org/10.5815/ijigsp.2009.01.01

[20] Tsai, D.-M. (1995). "A fast thresholding selection procedure for multimodal and unimodal histograms." Pattern Recognition Letters 16: 653-666.

[21] Baveye, P. C., Laba, M., Otten, W., Bouckaert, L., Dello Sterpaio, P., Goswami, R. R., … Sezgin, M. (2010). Observer-dependent variability of the thresholding step in the quantitative analysis of soil images and X-ray microtomography data. *Geoderma*, *157*(1–2), 51–63. https://doi.org/10.1016/j.geoderma.2010.03.015

[22] Carminati, A., Kaestner, A., Hassanein, R., Ippisch, O., Vontobel, P., & Flühler, H. (2007). Infiltration through series of soil aggregates: Neutron radiography and modeling. *Advances in Water Resources*, *30*(5), 1168–1178. https://doi.org/10.1016/j.advwatres.2006.10.006

[23] Culligan, K. A., Wildenschild, D., Christensen, B. S. B., Gray, W. G., & Rivers, M. L. (2006). Pore-scale characteristics of multiphase flow in porous media: A comparison of air-water and oil-water experiments. *Advances in Water Resources*, *29*(2), 227–238. https://doi.org/10.1016/j.advwatres.2005.03.021

[24] Jassogne, L., McNeill, A., & Chittleborough, D. (2007). 3D-visualization and analysis of macro- and meso-porosity of the upper horizons of a sodic, texture-contrast soil. *European Journal of Soil Science*, *58*(3), 589–598. https://doi.org/10.1111/j.1365-2389.2006.00849.x

[25] Kaestner, A., Lehmann, E., & Stampanoni, M. (2008). Imaging and image processing in porous media research. *Advances in Water Resources*, *31*(9), 1174–1187. https://doi.org/10.1016/j.advwatres.2008.01.022

[26] Kurita, T., Otsu, N., & Abdelmalek, N. (1992). Maximum Likelihood Thresholding Based on. *Pattern Recognition*, *25*(10), 1231–1240. https://doi.org/10.1016/0031-3203(92)90024-D

[27] Lee, S. S., Gantzer, C. J., Thompson, A. L., Anderson, S. H., and Ketcham, R. A. (2008). "Using High-Resolution Computed Tomography Analysis To Characterize Soil-Surface Seals Contribution of Missouri Agric." *Soil Science Society of America Journal*, 72(5), 1478-1485.

[28] Nunan, N., Ritz, K., Rivers, M., Feeney, D. S., & Young, I. M. (2006). Investigating microbial micro-habitat structure using X-ray computed tomography. *Geoderma*, *133*(3–4), 398–407. https://doi.org/10.1016/j.geoderma.2005.08.004

[29] Ojeda-Magaña, B., Quintanilla-Domínguez, J., Ruelas, R., Tarquis, A. M., Gómez-Barba, L., & Andina, D. (2014). Identification of pore spaces in 3D CT soil images using PFCM

partitional clustering. *Geoderma*, *217–218*, 90–101. https://doi.org/10.1016/j.geoderma.2013.11.005

[30] Ridler, T.W. Calvard, S. (1978). Picture Thresholding Using an Iterative Slection Method. *IEEE Transactions on Systems, Man and Cybernetics*, *8*(8), 630–632. https://doi.org/10.1109/TSMC.1978.4310039

[31] Schaap, M. G., Porter, M. L., Christensen, B. S. B., and Wildenschild, D. (2007). "Comparison of pressure-saturation characteristics derived from computed tomography and lattice Boltzmann simulations." *Water Resources Research*, 43(12), n/a-n/a.

[32] Schlüter, S., Weller, U., & Vogel, H. J. (2010). Segmentation of X-ray microtomography images of soil using gradient masks. *Computers and Geosciences*, *36*(10), 1246–1251. https://doi.org/10.1016/j.cageo.2010.02.007

[33] Van Geet, M., Lagrou, D., and Swennen, R. (2003). "Porosity measurements of sedimentary rocks by means of microfocus X-ray computed tomography (μCT)." In Mees, F., Swennen, R., Van Geet, M., and Jacobs, P. (eds) *Applications of X-ray computed tomography in the geosciences*. Geological Society, London, Special publications, 215, 51-60.

[34] Vogel, H.-J., Tölke, J., Schulz, V. P., Krafczyk, M., & Roth, K. (2005). Comparison of a Lattice-Boltzmann Model, a Full-Morphology Model, and a Pore Network Model for Determining Capillary Pressure–Saturation Relationships. *Vadose Zone Journal*, *4*(2), 380. https://doi.org/10.2136/vzj2004.0114

[35] Wildenschild, D., Vaz, C. M. P., Rivers, M. L., Rikard, D., and Christensen, B. S. B. (2002). "Using X-ray computed tomography in hydrology: systems, resolutions, and limitations." *Journal of Hydrology*, 267(3–4), 285-297.

[36] Mathworks. 2015. Matlab 2015,Mathworks Inc., Natick, MA.